Inorg. Chem. **2009**, *48*, 1744−1752

Complex Formation of Uranyl Ion with Triphenylphosphine Oxide and Its Ligand Exchange Reaction in 1-Butyl-3-methylimidazolium Nonafluorobutanesulfonate Ionic Liquid

Koichiro Takao,[†] Takafumi Takahashi,[‡] and Yasuhisa Ikeda*

Research Laboratory for Nuclear Reactors, Tokyo Institute of Technology, 2-12-1-N1-34, O-okayama, Meguro-ku, Tokyo 152-8550, Japan

Received September 30, 2008

Complex formation of the uranyl ion (UO_2^{2+}) with triphenylphosphine oxide ($OPPh_3$) in 1-butyl-3-methylimidazolium nonafluorobutanesulfonate ([BMI][NfO]) ionic liquid was investigated by means of ^{31}P NMR spectroscopy. In [BMI][NfO], coordination of $OPPh_3$ to UO_2^{2+} was found, and its coordination number was 4.1 ± 0.2, indicating $UO_2(OPPh_3)_4^{2+}$. From the [BMI][NfO] solution containing UO_2^{2+} and $OPPh_3$, yellow crystals of $UO_2(OPPh_3)_4(ClO_4)_2$ deposited, and its molecular and crystal structures were determined by using single-crystal X-ray analysis. An $OPPh_3$ exchange reaction of $UO_2(OPPh_3)_4^{2+}$ in [BMI][NfO] was also examined. The apparent first-order rate constant (k_{obs}) showed the first-order dependence on $[OPPh_3]$ ($k_{obs} = k_4[OPPh_3]_{free}$), suggesting the "associative" (A) mechanism. Its activation parameters were $\Delta H_4^{\ddagger} = 55.3 \pm 2.8$ kJ mol^{-1} and $\Delta S_4^{\ddagger} = 16.1 \pm 7.9$ J mol^{-1} K^{-1}. To compare the reactivity of $UO_2(OPPh_3)_4^{2+}$ in [BMI][NfO] with that in an ordinary organic solvent, the same reaction in CD_2Cl_2 was studied. In the CD_2Cl_2 system, an equilibrium between $UO_2(OPPh_3)_4^{2+}$ and $UO_2(OPPh_3)_5^{2+}$ was observed. The k_{obs} values of the $OPPh_3$ exchange reactions in $UO_2(OPPh_3)_4^{2+}$ (k_{4obs}) and $UO_2(OPPh_3)_5^{2+}$ (k_{5obs}) in CD_2Cl_2 are expressed as $k_{4obs} = k_4[OPPh_3]_{free}$ and $k_{5obs} = k_5$, respectively, indicating that the exchange reactions in $UO_2(OPPh_3)_4^{2+}$ and $UO_2(OPPh_3)_5^{2+}$ are categorized in A and "dissociative" (D) mechanisms, respectively. The activation parameters of these reactions were also estimated ($UO_2(OPPh_3)_4^{2+}$: $\Delta H_4^{\ddagger} = 7.1 \pm 0.3$ kJ mol^{-1} and $\Delta S_4^{\ddagger} = -122 \pm 1$ J mol^{-1} K^{-1}, $UO_2(OPPh_3)_5^{2+}$: $\Delta H_5^{\ddagger} = 62.4 \pm 1.0$ kJ mol^{-1} and $\Delta S_5^{\ddagger} = 68.4 \pm 4.2$ J mol^{-1} K^{-1}). A large difference in the reactivity of $UO_2(OPPh_3)_4^{2+}$ was found between [BMI][NfO] and CD_2Cl_2. This was explained by the formation of a specific solvation barrier of NfO^- around $UO_2(OPPh_3)_4^{2+}$ in [BMI][NfO].

1. Introduction

Ionic liquids (ILs) consist of only ionic species and have characteristic properties: a low melting point, nonvolatility, nonflammability, high conductivity, a wide electrochemical potential window, and so on. Because of these properties, ILs have been noted as alternative media in various fields, for example, organic synthesis,[1−5] electrochemical devices,[6] and nuclear engineering.[7−10] One of the most important elements in nuclear engineering is uranium, of which the most stable oxidation state is +6, that is, the uranyl ion (UO_2^{2+}). Indeed, the complex formation, structure, electrochemistry, and extraction behavior of UO_2^{2+} and its complexes in several ILs have been studied.[9−17]

* To whom correspondence should be addressed. E-mail: yikeda@nr.titech.ac.jp.

[†] This author's last name has been changed from Mizuoka. Present address: Institute of Radiochemistry, Forschungszentrum Dresden-Rossendorf (FZD), Germany. E-mail: k.takao@fzd.de.

[‡] Present address: Advanced Technology Research Laboratories, Nippon Steel Corporation. E-mail: takahashi.takafumi@nsc.co.jp.

(1) Olivier-Bourbigou, H.; Magna, L *J. Mol. Catal. A: Chem.* **2002**, *182−183*, 419–437.
(2) Earle, M. J.; Seddon, K. R. *Pure Appl. Chem.* **2000**, *72*, 1391–1398.
(3) Wasserscheid, P.; Keim, W. *Angew. Chem., Int. Ed.* **2000**, *39*, 3772–3789.
(4) Welton, T. *Chem. Rev.* **1999**, *99*, 2071–2083.
(5) Dupont, J.; De Souza, R. F.; Suarez, P. A. Z. *Chem. Rev.* **2002**, *102*, 3667–3692.
(6) Bonhote, P.; Dias, A.-P.; Papageorgiou, N.; Kalyanasundaram, K.; Grätzel, M. *Inorg. Chem.* **1996**, *35*, 1168–1178.
(7) Bradley, A. E.; Hatter, J. E.; Nieuwenhuyzen, M.; Pitner, W. R.; Seddon, K. R.; Thied, R. C. *Inorg. Chem.* **2002**, *41*, 1692–1694.
(8) Bradley, A. E.; Hardacre, C.; Nieuwenhuyzen, M.; Pitner, W. R.; Sanders, D.; Seddon, K. R.; Thied, R. C. *Inorg. Chem.* **2004**, *43*, 2503–2514.
(9) Visser, A. E.; Jensen, M. P.; Laszak, I.; Nash, K. L.; Choppin, G. R.; Rogers, R. D. *Inorg. Chem.* **2003**, *42*, 2197–2199.

10.1021/ic8018666 CCC: $40.75
Published on Web 01/12/2009

Solution chemists will be interested in the solvation around a metal ion (M^{n+}) in IL, complex formation of M^{n+} with ligands in IL, and the difference in reactivity of M^{n+} between IL and other ordinary solvents. These matters are not only of great interest in basic solution chemistry but also impotant in the applications of ILs as nobel reaction fields. In recent years, such chemistry of M^{n+} in ILs has been developed, for instance, lanthanides and actinides reviewed by Binnemans[16] and Cocalia et al.[17] However, the kinetics and thermodynamics of M^{n+} in ILs are not explored sufficiently.[5] One can find only a few cases of kinetic studies in ILs.[18−21] Especially for ligand exchange reactions in ILs, there seem to be no reports in spite of the importance of the kinetic information of this simplest reaction with $\Delta G^\circ = 0$ being an indicator to know the reactivity of M^{n+} in a medium of interest.[22,23] In this situation, we recently studied the kinetics of a complexation reaction of Li^+ with cryptand C211 in two different ILs using ^{7}Li NMR spectroscopy.[24] As a result, several differences in the reaction rate and mechanism of the complexation reaction in the Li^+−C211 system were discovered between ILs and organic solvents (dimethyl sulfoxide, *N*,*N*-dimethylformamide).

Nuclear magnetic resonance (NMR) is frequently utilized as one of the powerful techniques to study metal−ligand complexation and its ligand exchange reactions.[22,23,25,26] However, nuclides in the investigation of IL samples using NMR will be strictly restricted.[27] It is difficult to use the most popular and most abundant nuclide, ^{1}H, because deuterated ILs are not supplied sufficiently. Furthermore, ^{13}C and ^{19}F are also components of most ILs. Thus, it is also not easy to adopt these nuclides as targets in the NMR experiments. The remaining NMR-observable nuclides are ^{2}D, ^{15}N, ^{17}O, ^{31}P, ^{35}Cl, and so on. On the basis of natural abundance and NMR sensitivity, we reached a conclusion that ^{31}P seems to be the most suitable. In this study, we selected triphenylphosphine oxide ($OPPh_3$) as a ligand including ^{31}P. This ligand has been known to coordinate to UO_2^{2+} strongly.[28,29] Previously, we studied the chemical form around UO_2^{2+} in 1-butyl-3-methylimidazolium nonafluorobutanesulfonate ([BMI][NfO], Chart 1) and found that $UO_2(H_2O)_n^{2+}$ can be dehydrated by heating under reduced pressure.[12] Experimental facts from Raman, ^{35}Cl NMR, and absorption spectroscopies suggested that there is no remarkable coordination in the equatorial plane of UO_2^{2+} in [BMI][NfO] after the dehydration, that is, "bare" UO_2^{2+}. Although the structure around UO_2^{2+} in [BMI][NfO] should be investigated in detail, coordination of $OPPh_3$ to UO_2^{2+} in [BMI][NfO] was expected to proceed without any complication. Our goals here are to confirm if UO_2^{2+} and $OPPh_3$ form a complex even in [BMI][NfO] and to obtain the kinetic information of the ligand exchange reaction in this IL. To compare the reactivity of UO_2^{2+} in IL, we also studied the same reaction in the ordinary noncoordinating organic solvent, CD_2Cl_2.

Chart 1

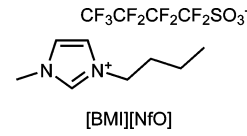

[BMI][NfO]

2. Experimental Section

1-Butyl-3-methylimidazolium nonafluorobutanesulfonate ([BMI][NfO]) was synthesized using the following procedure. 1-Butyl-3-methylimidazolium bromide ([BMI][Br]) was prepared by refluxing a mixture of 1-methylimidazole (MIm, Kanto Chemical Co., Ind.) and 1-bromobutane (*n*BuBr, Kanto, 10 mol % excess) in tetrahydrofuran (THF). With progress in the reaction between MIm and *n*BuBr, the solution became turbid and finally formed two layers after 2 h. The upper THF layer was removed by decantation. Any volatiles in the lower [BMI][Br] layer were evaporated under reduced pressure. All chemicals were of reagent grade and used as received.

A parent salt of NfO^- was potassium nonafluorobutanesulfonate (KNfO, JEMCO KFBS EF-42). This compound was twice recrystalized from boiling water (ca. 50 wt %) and then dried on a hot plate until the formation of fine white powder of KNfO was achieved. The obtained [BMI][Br] was dissolved in distilled water and mixed with an equivalent molar amount of KNfO. This mixture was heated with vigorous stirring for 2 h, followed by cooling to room temperature. The lower [BMI][NfO] layer was separated. The impurities in [BMI][NfO] were removed through washing with distilled water six times and contact with activated charcoal. Water in [BMI][NfO] was evaporated by heating at 120 °C under reduced pressure. Excess KNfO was removed through the dissolution of [BMI][NfO] in CH_2Cl_2 and filtration. Dichloromethane in the filtrate was evaporated with heating under reduced pressure. The residue was obtained as the purified [BMI][NfO], which was a viscous colorless liquid. The purity of the obtained [BMI][NfO] was confirmed by ^{1}H and ^{19}F NMR spectroscopy.[12]

(10) Ouadi, A.; Klimchuk, O.; Gaillard, C.; Billard, I. *Green Chem.* **2007**, *9*, 1160–1162.
(11) Hopkins, T. A.; Berg, J. M.; Costa, D. A.; Smith, W. H.; Dewey, H. J. *Inorg. Chem.* **2001**, *40*, 1820–1825.
(12) Mizuoka, K.; Ikeda, Y. *Prog. Nucl. Energy* **2005**, *47*, 426–433.
(13) Gaillard, C.; Chaumont, A.; Billard, I.; Hennig, C.; Ouadi, A.; Wipff, G. *Inorg. Chem.* **2007**, *46*, 4815–4826.
(14) Nockemann, P.; Servaes, K.; van Deun, R.; van Hecke, K.; van Meervelt, L.; Binnemans, K.; Görller-Walrand, C. *Inorg. Chem.* **2007**, *46*, 11335–11344.
(15) Bossé, E.; den Auwer, C.; Berthon, C.; Guilbaud, P.; Vrigoriev, M. S.; Nikitenko, S.; le Naour, C.; Cannes, C.; Moisy, P. *Inorg. Chem.* **2008**, *47*, 5746–5755.
(16) Binnemans, K. *Chem. Rev.* **2007**, *107*, 2592–2614.
(17) Cocalia, V. A.; Gutowski, K. E.; Rogers, R. D. *Coord. Chem. Rev.* **2006**, *250*, 755–764.
(18) Müller, L. A.; Dupont, J.; de Souza, R. F. *Macromol. Rapid Commun.* **1998**, *19*, 409–411.
(19) Durazo, A.; Abu-Omar, M. M. *Chem. Commun.* **2002**, 66–67.
(20) Weber, C. F.; Puchta, R.; van Eikema Hommes, N. J. R.; Wasserscheid, P.; van Eldik, R. *Angew. Chem., Int. Ed.* **2005**, *44*, 6033–6038.
(21) Illner, P.; Kern, S.; Begel, S.; van Eldik, R. *Chem. Commun.* **2007**, 4803–4805.
(22) Dunand, F. A.; Helm, L.; Merbach, A. E. *Adv. Inorg. Chem.* **2003**, *54*, 1–69.
(23) Helm, L.; Merbach, A. E. *Chem. Rev.* **2005**, *105*, 1923–1959.
(24) Shirai, A.; Ikeda, Y. *Chem. Lett.* **2008**, *37*, 552–553.
(25) Lincoln, S. F. *Prog. React. Kinet.* **1977**, *9*, 1–91.
(26) Giernoth, R.; Bankmann, D.; Schlörer, N. *Green Chem.* **2005**, *7*, 279–282.
(27) Bankmann, D.; Giernoth, R. *Prog. Nucl. Magn. Reson. Spectrosc.* **2007**, *51*, 63–90.
(28) Berthet, J.-C.; Nierlich, M.; Ephritikhine, M. *Angew. Chem., Int. Ed.* **2003**, *42*, 1952–1954.
(29) John, G. H; May, I; Sarsfield, M. J; Steele, H. M; Collison, D; Helliwell, M; McKinney, J. D. *Dalton Trans.* **2004**, 734–740.

Uranyl perchlorate hydrate ($UO_2(ClO_4)_2 \cdot nH_2O$, $n \simeq 5$) was prepared by dissolving UO_3 in $HClO_4$(aq). This solution was concentrated to near dryness. To remove excess acid in $UO_2(ClO_4)_2 \cdot nH_2O$, the addition of a small amount of distilled water and evaporation with heating were repeated until no white fume was observed.

The uranyl perchlorate salt was dissolved in [BMI][NfO], and the hydrated water was removed by evaporation at 120 °C under reduced pressure. The completion of the dehydration from UO_2^{2+} was confirmed by ^{1}H NMR and UV−visible absorption spectroscopy.[12] To this solution, a calculated amount of $OPPh_3$ (Kanto) was added. After the dissolution of $OPPh_3$ with heating under reduced pressure, the ^{31}P NMR spectra of [BMI][NfO] containing UO_2^{2+} and $OPPh_3$ were recorded at different temperatures with the ^{1}H decoupling mode using the JEOL JNM-LA300WB FT NMR system (^{1}H, 300.40 MHz; ^{31}P, 121.50 MHz). In this article, the chemical shifts in all ^{31}P NMR spectra are reported versus 85% H_3PO_4 as an external reference.

For CD_2Cl_2 systems, $UO_2(OPPh_3)_4(ClO_4)_2$ was prepared as a starting material by mixing $UO_2(ClO_4)_2 \cdot nH_2O$ and $OPPh_3$ in ethanol. Calculated amounts of $UO_2(OPPh_3)_4(ClO_4)_2$ and $OPPh_3$ were dissolved in CD_2Cl_2. For this sample, the ^{31}P NMR spectra were measured at various temperatures with the ^{1}H decoupling mode using a JEOL ECX-400 NMR spectrometer (^{1}H, 399.78 MHz; ^{31}P, 161.83 MHz).

Caution! *Perchlorate salts are potentially explosive. Handling of all compounds containing perchlorate, especially for heating $UO_2(ClO_4)_2 \cdot nH_2O$, should be done with great care and in small amounts.*

Kinetic analyses for ligand exchange reactions in the UO_2^{2+}−$OPPh_3$ complex were performed using the NMR line-broadening method.[25,30] The full line width at the half-maximum ($\Delta\nu$) of each spectrum was obtained by Lorentz deconvolution using Igor Pro 5.05J.[31] To simulate the NMR spectrum involving the ligand exchange phenomenon, the computer program gNMR[32] was utilized. The apparent first-order rate constant (k_{obs}) in each NMR spectrum was estimated by iterating the spectrum simulation in gNMR to fit the observed spectra in the exchange systems which follow the simple two-site model. Otherwise, k_{obs} was calculated from the $\Delta\nu$ of coordinated $OPPh_3$, as described elsewhere.[30] In the spectrum fitting by gNMR, a constant line width of the coordinated $OPPh_3$ in the absence of chemical exchange, $\Delta\nu_{m0} =$ 250 Hz, was subtracted from each spectrum of the [BMI][NfO] solution. This quantity was calculated from the following relationship under the *slow exchange limit*.[25]

$$\Delta\nu_{m0} = \Delta\nu_m - \frac{k_{obs}}{\pi} \quad (1)$$

The term, k_{obs}/π, is expressed by the $\Delta\nu$ of the free $OPPh_3$ in the presence and absence of chemical exchange ($\Delta\nu_f$ and $\Delta\nu_{f0}$, respectively) as follows:

$$\frac{k_{obs}}{\pi} = (\Delta\nu_f - \Delta\nu_{f0})\frac{P_m}{P_f} \quad (2)$$

where P_m and P_f are the fractions of the coordinated and free $OPPh_3$, respectively. From the ^{31}P NMR spectrum of the free $OPPh_3$ in [BMI][NfO] shown in Figure S1 in the Supporting Information, $\Delta\nu_{f0}$ was evaluated as 33 Hz. We first calculated k_{obs}/π at several temperatures under the *slow exchange limit* by using eq 2 and then estimated $\Delta\nu_{m0}$ from eq 1. The resulting $\Delta\nu_{m0}$ was almost constant at 250 ± 15 Hz. The agreement of the k_{obs} from the gNMR fitting with those from eq 2 was also confirmed.

Table 1. Crystallographic Data of $UO_2(OPPh_3)_4(ClO_4)_2$ Deposited from [BMI][NfO]

formula	$C_{72}H_{60}Cl_2O_{14}P_4U$	Z	2
fw	1582.01	T (K)	173
cryst size (mm)	0.20 × 0.15 × 0.15	D_{calcd} (g cm^{-1})	1.565
cryst syst	monoclinic	μ (mm^{-1})	2.657
space group	$P2_1/c$ (#14)	obsd. data	7624
a (Å)	9.728(5)	R^a ($I > 2\sigma$)	0.0487
b (Å)	24.98(1)	wR^b (all)	0.1100
c (Å)	13.990(9)	GOF^c	1.054
β (deg)	99.64(5)	$\Delta\rho_{max}$ (e$^-$ Å^{-3})	1.480
V (Å^3)	3358(3)	$\Delta\rho_{min}$ (e$^-$ Å^{-3})	−0.951

^{a} $R = \sum ||F_o| - |F_c|| / \sum |F_o|$. ^{b} $wR = [\sum w(F_o^2 - F_c^2)^2 / \sum w(F_o^2)^2]^{1/2}$, ^{c} GOF $= [\sum w(F_o^2 - F_c^2)^2/(N_o - N_c)]^{1/2}$. Detailed values of the weight (w) is given in the crystallographic information file provided as Supporting Information.

Single Crystal X-Ray Analysis. From the dissolved $UO_2(ClO_4)_2$ and $OPPh_3$ in [BMI][NfO] solution, some yellow crystals were deposited. A single crystal of this compound was mounted on a glass capillary and put into a temperature-controlled nitrogen gas stream (173 K). Intensity data were collected by using an imaging plate area detector in Rigaku RAXIS RAPID with graphite monochromated Mo Kα radiation ($\lambda = 0.71075$ Å). The structure was solved by a direct method, SIR92,[33] and expanded using Fourier techniques.[34] A numerical absorption correction was applied and resulted in transmission factors described in the crystallographic information file.[35] All non-hydrogen atoms were anisotropically refined by SHELXL-97.[36] Hydrogen atoms were refined as riding on their parent atoms with U_{iso} (H) = 1.2U_{eq} (C). The final cycle of full-matrix least-squares refinement on F^2 was based on observed reflections and parameters and converged with the unweighted and weighted agreement factors, R and wR. All calculations were performed by the CrystalStructure crystallographic software package.[37] Crystallographic data and other data collection parameters are summarized in Table 1.

Determination of Self-Diffusion Coefficient of BMI^+. A ^{1}H pulsed-field gradient spin−echo (PGSE) method was utilized to determine a self-diffusion coefficient of BMI^+ (D_{BMI}) in [BMI][NfO]. This experiment was carried out at 297 ± 0.5 K using an Apollo spectrometer operating at a resonance frequency of 300 MHz for ^{1}H with a 7.01 T superconducting electromagnet. Details of the experimental procedure were described in our previous article.[38] The observed echo attenuation (I/I_0) is expressed as

$$I/I_0 = \exp(-D_{BMI}b) \quad (3)$$

$$b = \frac{\gamma^2 g^2 \delta^2 (4\Delta - \delta)}{\pi^2} \quad (4)$$

where γ, g, δ, and Δ are the ^{1}H magnetogyric ratio (2.675 × 10^8 rad T^{-1}), the strength of the field gradient pulses, the duration of

(30) Takao, K.; Ikeda, Y. *Inorg. Chem.* **2007**, *46*, 1550–1562.
(31) *Igor Pro*, ver. 5.05J; Wavemetrics, Inc.: Lake Oswego, OR.
(32) *gNMR*, ver. 5.0.4.0; Adept Scientific, Inc.: Bethesda, MD.
(33) Altomare, A.; Cascarano, G.; Giacovazzo, C.; Guagliardi, A. *J. Appl. Crystallogr.* **1993**, *26*, 343–350.
(34) Beurskens, P. T.; Admiraal, G.; Beurskens, G.; Bosman, W. P.; Gelder, de R.; Israel, R.; Smits, J. M. M. *DIRDIF99*; Technical Report of the Crystallography Laboratory, University of Nijmegen: Nijmegen, The Netherlands, 1999.
(35) Higashi, T. *NUMABS*; Rigaku Corporation: Tokyo, Japan, 1999.
(36) Sheldrick, G. M, *SHELXL-97*; University of Göttingen: Göttingen, Germany, 1997.
(37) *Crystal Structure 3.10*; Rigaku and Rigaku/MSC: Tokyo, Japan, 2000−2002.
(38) Takahashi, T.; Ohkubo, T.; Ikeda, Y. *J. Colloid Interface Sci.* **2006**, *299*, 198–203.

the field gradient pulses, and the interval between two gradient pulses, respectively.[39] The parameters used here are $0 < g < 184$ G cm^{-1}, $\delta = 6.0$ ms, and $\Delta = 58.64$ ms. The D_{BMI} value was determined by the least-squares fit of eq 3 to the experimental data.

3. Results and Discussion

3.1. Complex Formation of UO_2^{2+} with $OPPh_3$ in [BMI][NfO]. To investigate how UO_2^{2+} forms a complex with $OPPh_3$ in [BMI][NfO], the ^{31}P NMR spectrum of a solution of $UO_2(ClO_4)_2$ (6.07×10^{-2} M) and $OPPh_3$ (total 6.26×10^{-1} M) dissolved in [BMI][NfO] was recorded. The observed spectrum at 283 K is shown in Figure 1. As can be seen from this figure, two singlet signals are detected at 28.4 and 53.3 ppm. The former corresponds to the ^{31}P NMR signal of free $OPPh_3$ in [BMI][NfO] (Figure S1 in the Supporting Information), and the latter is attributable to that of $OPPh_3$ coordinated to UO_2^{2+}. From the peak integrals of these signals, the coordination number of $OPPh_3$ to UO_2^{2+} was evaluated as 4.1 ± 0.2.

From the [BMI][NfO] solution used in Figure 1, yellow crystals were grown slowly during its storage for several months. To determine molecular and crystal structures of this yellow crystal, single-crystal X-ray analysis was performed. As a result, it was clarified that this crystal is $UO_2(OPPh_3)_4(ClO_4)_2$. The molecular structure, crystallographic data, and selected structural parameters of $UO_2(OPPh_3)_4(ClO_4)_2$ obtained from [BMI][NfO] are shown in Figure 2 and Tables 1 and 2, respectively. As seen from Figure 2, the uranium atom is surrounded by four oxygen atoms from $OPPh_3$ in the equatorial plane (O_L) and coordinated by two axial oxygen atoms (O_{yl}). The bond distances in U$-O_{yl}$ and U$-O_L$ are 1.758(4) and 2.30 Å (mean), respectively. The bond angles around U in all directions (i.e., $\angle O_{yl}-U-O_L$, $\angle O_L-U-O_L$) are close to 90°. Thus, the coordination geometry around U is tetragonal bipyramidal in D_{4h} symmetry. The crystal structure of $UO_2(OPPh_3)_4(ClO_4)_2$ obtained from [BMI][NfO] seems not to be unique. The same crystals were also obtained from a solution of $UO_2(ClO_4)_2 \cdot 5H_2O$ and $OPPh_3$ dissolved in ethanol at a 1:4 ratio (Figure S2, Supporting Information).

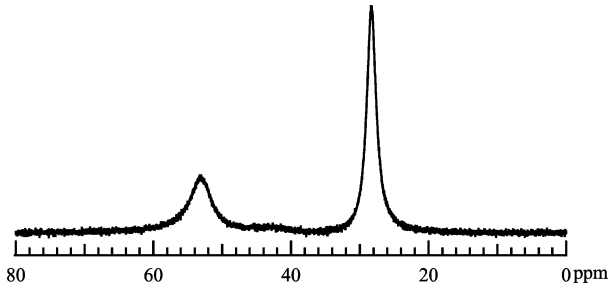

Figure 1. $^{31}P\{^1H\}$ NMR spectrum of [BMI][NfO] solution dissolving $UO_2(ClO_4)_2$ (6.07×10^{-2} M) and $OPPh_3$ (total: 6.26×10^{-1} M) at 283 K.

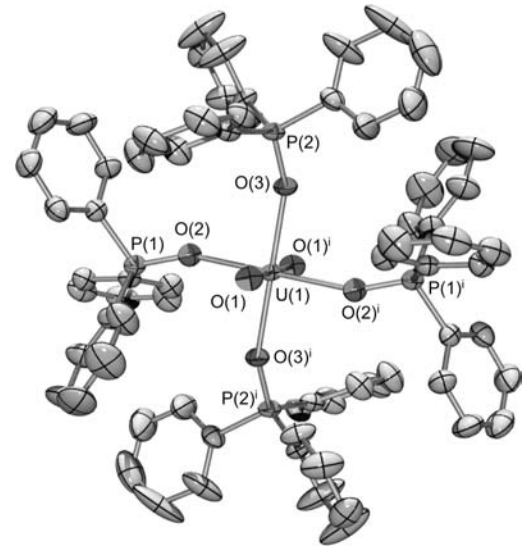

Figure 2. ORTEP drawing of $UO_2(OPPh_3)_4^{2+}$ in the ClO_4^- salt deposited from a [BMI][NfO] solution at the 50% probability level. Hydrogen atoms and ClO_4^- are omitted for clarity. Symmetry code: (i) $-x, 1-y, 1-z$.

Table 2. Selected Structural Parameters of $UO_2(OPPh_3)_4(ClO_4)_2$ Deposited from [BMI][NfO]

Bond Length (Å)			
U(1)−O(1)	1.758(4)	P(1)−O(2)	1.528(4)
U(1)−O(2)	2.287(4)	P(2)−O(3)	1.516(4)
U(1)−O(3)	2.310(4)		
Bond Angles (deg)			
O(1)−U(1)−O(2)	90.5(2)	U(1)−O(2)−P(1)	155.3(3)
O(1)−U(1)−O(3)	90.3(2)	U(1)−O(3)−P(2)	156.8(3)
O(2)−U(1)−O(3)	89.9(1)		

On the basis of the consistency between the coordination number of $OPPh_3$ in the [BMI][NfO] solution and the crystal, $UO_2(OPPh_3)_4^{2+}$ is also present in [BMI][NfO]. On the other hand, the coordination of NfO^- might be possible. Actually, we reported that UO_2^{2+} forms a complex with NfO^- and THF, that is, $UO_2(NfO)_2(THF)_3$, in our recent publication.[40] However, the bond length between U and O of NfO^- in $UO_2(NfO)_2(THF)_3$ is 2.388(5) Å, which is ca. 0.1 Å longer than the U$-O_L$ distance in $UO_2(OPPh_3)_4(ClO_4)_2$. Thus, the coordination of NfO^- to U will not be as strong as that of $OPPh_3$. This suggestion is reasonable from the viewpoint of the strongest electronegativity of fluorine atoms in NfO^-; that is, electron density on the O atoms in NfO^- should be decreased by the strongest electron-withdrawing nature of the F atoms. If the NfO^- coordination is present in the solution of Figure 1, its exchange reaction with the bulk NfO^- should occur. Under slow exchange conditions, two ^{31}P signals of coordinated $OPPh_3$ nearer to and farther from coordinated NfO^- will be observed, being contradictory to Figure 1. Even if such a NfO^- exchange reaction rate is fast, the temperature dependence of the spectra could be no longer treated as a simple two-site model as described below. Additionally, the ^{31}P chemical shift of the coordinated $OPPh_3$ in [BMI][NfO] (53.3 ppm) well agrees with that of $UO_2(OPPh_3)_4^{2+}$ in the noncoordinating CD_2Cl_2 (53.0 ppm,

(39) Price, W. S.; Hayamizu, K.; Ide, H.; Arata, Y. *J. Magn. Reson.* **1999**, *139*, 205–212.
(40) Takao, K.; Ikeda, Y. *Acta Crystallogr.* **2008**, *E64*, m168.

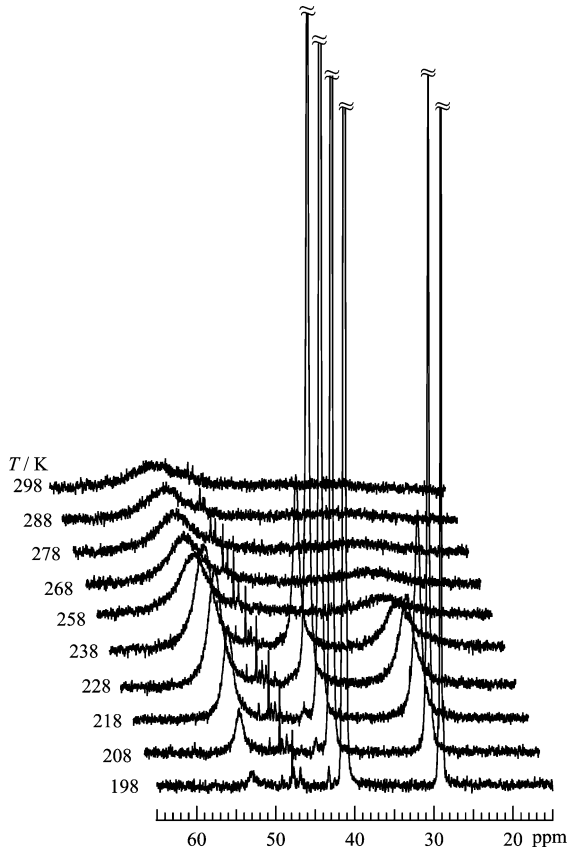

Figure 3. $^{31}P\{^1H\}$ NMR spectra of CD_2Cl_2 solution dissolving $UO_2(OPPh_3)_4(ClO_4)_2$ (1.33×10^{-2} M) and $OPPh_3$ (2.79×10^{-2} M at initial) recorded at various temperatures.

Figure 3, details are described below). Therefore, the NfO^- coordination should not occur in the [BMI][NfO] solution of Figure 1. In conclusion, UO_2^{2+} is present as $UO_2(OPPh_3)_4^{2+}$ in the [BMI][NfO] solution, and its molecular structure is similar to that shown in Figure 2.

3.2. $UO_2(OPPh_3)_4^{2+}$ in [BMI][NfO] with Free $OPPh_3$. In the presence of both $UO_2(OPPh_3)_4^{2+}$ and free $OPPh_3$ in [BMI][NfO], the following $OPPh_3$ exchange reaction is expected to take place:

$$UO_2(OPPh_3)_4^{2+} + OPPh_3^* \rightarrow UO_2(OPPh_3)_3(OPPh_3^*)^{2+} + OPPh_3 \quad (5)$$

where the asterisk on $OPPh_3$ is typographical distinction only. In order to calculate the kinetic and the activation parameters for the exchange reaction in eq 5, we measured the ^{31}P NMR spectra of the [BMI][NfO] solution containing $UO_2(OPPh_3)_4^{2+}$ (6.07×10^{-2} M) and free $OPPh_3$ (3.83×10^{-1} M) at various temperatures (T). The results are shown in Figure 4a. With elevating T, the ^{31}P NMR signals of the coordinated and free $OPPh_3$ broaden and finally coalesce with each other. This phenomenon indicates that eq 5 takes place in [BMI][NfO].

The apparent first-order rate constant k_{obs} of eq 5 in each spectrum of Figure 4a was evaluated using the two-site model. The best fits for the observed spectra are shown in Figure 4b together with the refined k_{obs}. The similar experiments and analyses were performed at $[OPPh_3]_{free} = 2.44 \times 10^{-2}$, 7.88×10^{-2}, and 1.93×10^{-1} M. The obtained k_{obs} values were plotted in Figure 5 against the reciprocal T. As seen from this figure, k_{obs} clearly increases with an increase in $[OPPh_3]_{free}$. In Figure 6, k_{obs} values at each T are plotted as a function of $[OPPh_3]_{free}$. From this figure, the k_{obs} at each T is proportional to the first-order of $[OPPh_3]_{free}$ with a negligibly small intercept in the range of $[OPPh_3]_{free}$ examined here. Therefore, k_{obs} can be expressed as

$$k_{obs} = k_4[OPPh_3]_{free} \quad (6)$$

where k_4 is the second-order rate constant.

Equation 6 implies that the reaction mechanism of eq 5 is classified in so-called "associative" (A) and "interchange" (I) mechanisms or their combination (A + I).[22,23] If eq 5 in [BMI][NfO] proceeds through the I mechanism, k_{obs} is expressed as

$$k_{obs} = \frac{k_I K_{OS}[OPPh_3]_{free}}{1 + K_{OS}[OPPh_3]_{free}} \quad (7)$$

where k_I and K_{OS} are the rate constant of the I mechanism and the formation constant of an outer-sphere complex between $UO_2(OPPh_3)_4^{2+}$ and $OPPh_3$, respectively. Under the limiting conditions

$$1 \gg K_{OS}[OPPh_3]_{free} \quad k_{obs} \simeq k_I K_{OS}[OPPh_3]_{free} \quad (8)$$

$$1 \ll K_{OS}[OPPh_3]_{free} \quad k_{obs} \simeq k_I \quad (9)$$

These expressions indicate that k_{obs} proportionally increases with an increase in $[OPPh_3]_{free}$ at low $[OPPh_3]_{free}$, while it approaches the constant k_I at high $[OPPh_3]_{free}$. This is also the case for the (A + I) mechanism, where k_{obs} is given as

$$k_{obs} = \frac{(k_A + k_I K_{OS})[OPPh_3]_{free}}{1 + K_{OS}[OPPh_3]_{free}} \quad (10)$$

where k_A is the rate constant of the A mechanism. Under the limiting conditions

$$1 \gg K_{OS}[OPPh_3]_{free} \quad k_{obs} \simeq (k_A + k_1 K_{OS})[OPPh_3]_{free} \quad (11)$$

$$1 \ll K_{OS}[OPPh_3]_{free} \quad k_{obs} \simeq \frac{k_A + k_1 K_{OS}}{K_{OS}} \quad (12)$$

On the other hand, k_{obs} in the A mechanism is simply written as eq 6. As seen from Figure 6, k_{obs} shows the first-order dependence on $[OPPh_3]_{free}$ and does not approach a constant in spite of 15.7-fold variation of $[OPPh_3]_{free}$ (2.44×10^{-2} to 3.83×10^{-1} M). Therefore, the reaction mechanism of eq 5 in [BMI][NfO] should be classified in the A mechanism rather than I and A + I, that is, the rate-determining step of eq 5 in [BMI][NfO] is

$$UO_2(OPPh_3)_4^{2+} + OPPh_3 \xrightarrow{k_4} UO_2(OPPh_3)_5^{2+} \quad (13)$$

The k_4 value under each condition was calculated from the k_{obs} in Figure 5 using eq 6 and plotted against T^{-1} in Figure 7. In this figure, no significant dependence of k_4 on $[OPPh_3]_{free}$ is confirmed, indicating the validity of eq 6. Using the Eyring relationship (eq S1 in the Supporting Information), the activation enthalpy ($\Delta H_4^{\ddagger}$) and entropy ($\Delta S_4^{\ddagger}$) of eq 5

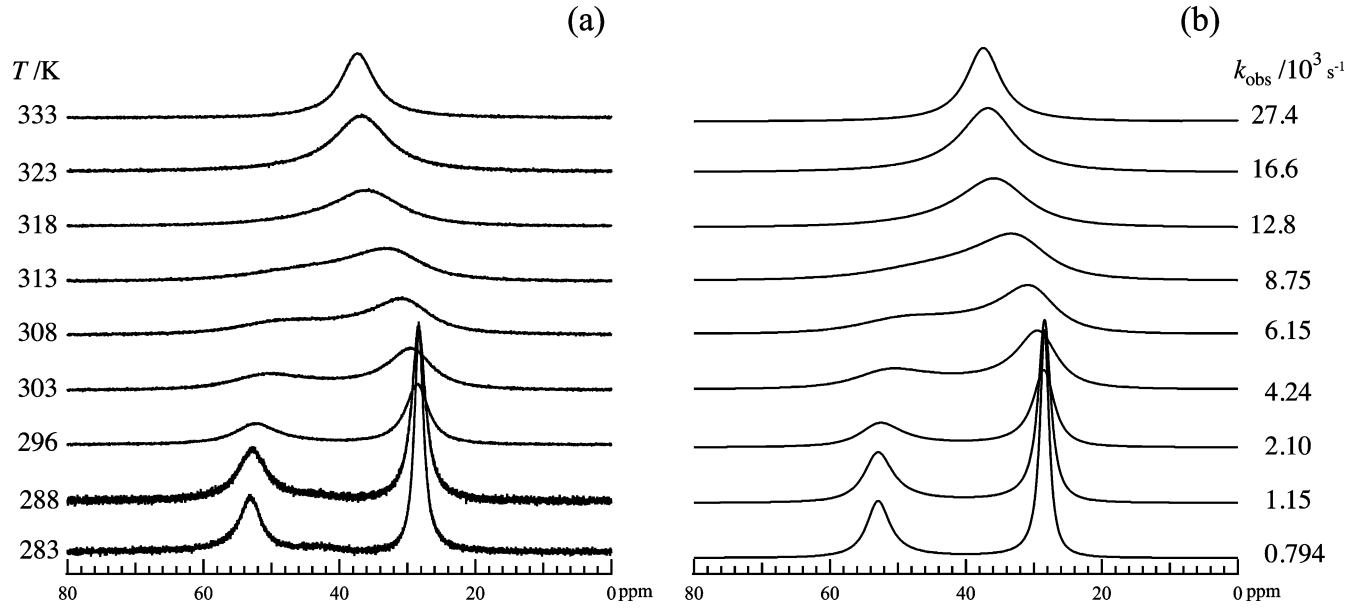

Figure 4. $^{31}P\{^1H\}$ NMR spectra of a [BMI][NfO] solution containing $UO_2(OPPh_3)_4^{2+}$ (6.07×10^{-2} M) and free $OPPh_3$ (3.83×10^{-1} M) recorded at various temperatures (a) and the best fits with different reaction rates simulated by gNMR (b).

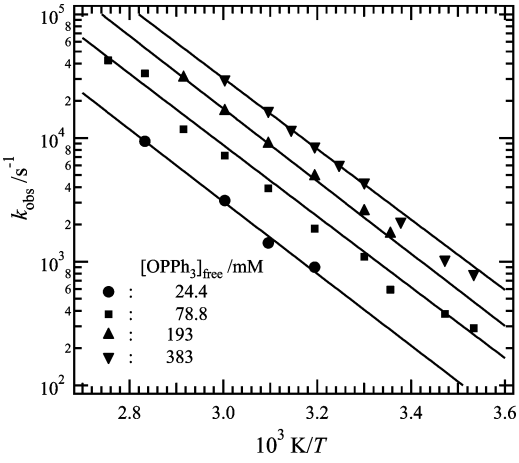

Figure 5. Temperature dependence of k_{obs} of eq 5 in a [BMI][NfO] solution. The smooth line for each data set is the best fit of the Eyring relationship (eq S1, Supporting Information).

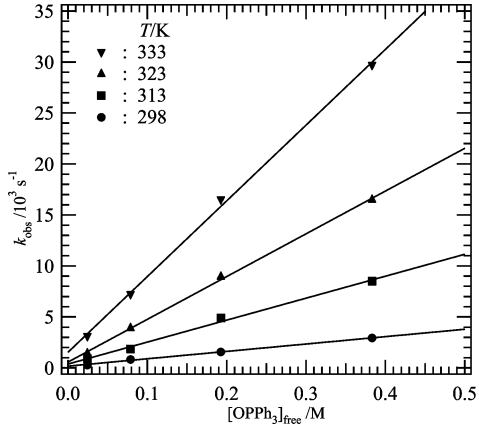

Figure 6. $[OPPh_3]_{free}$ dependence of k_{obs} of eq 5 in a [BMI][NfO] solution.

were calculated as 55.3 ± 2.8 kJ mol^{-1} and 16.1 ± 7.9 J mol^{-1} K^{-1}, respectively. From Figure 6, k_4 at 298 K was evaluated as (7.2 ± 0.3) × 10^3 M^{-1} s^{-1}. This is the first

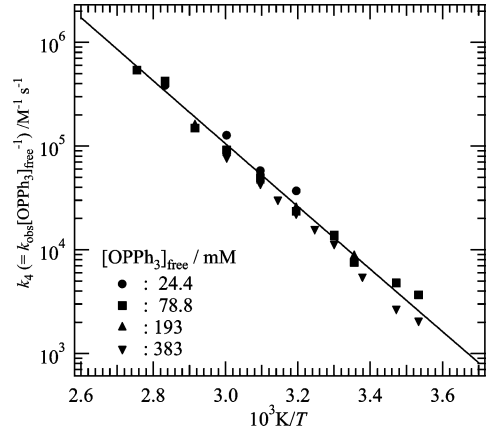

Figure 7. Temperature dependence of k_4 calculated from k_{obs} of Figure 5. Smooth line is the best fit of the Eyring relationship (eq S1) to the experimental data.

information given for the ligand exchange kinetics of UO_2^{2+} complexes in ILs.

3.3. $UO_2(OPPh_3)_n^{2+}$ in CD_2Cl_2 with Free $OPPh_3$ (n = 4, 5). To compare the reactivity of $UO_2(OPPh_3)_4^{2+}$ in [BMI][NfO] with that in an ordinary solvent, the ^{31}P NMR spectra of the solution of $UO_2(OPPh_3)_4(ClO_4)_2$ (1.33×10^{-2} M) and free $OPPh_3$ (2.79×10^{-2} M at initial) dissolved in CD_2Cl_2 were recorded at 198−298 K. The results are shown in Figure 3. In this figure, three signals were detected at 29.1, 41.4, and 53.0 ppm at 198 ≤ T ≤ 238 K, while two signals were observed at 29.1 and 53.0 ppm at T ≥ 258 K. The signal at 29.1 ppm is assigned to the free $OPPh_3$ in a comparison between Figure 3 and the spectrum of $OPPh_3$ in CD_2Cl_2 (Figure S1, Supporting Information). The remaining two signals at 41.4 and 53.0 ppm are attributable to the UO_2^{2+}−$OPPh_3$ complexes with different coordination numbers. Since the presence of the species at 41.4 ppm is negligible at T ≥ 258 K, the coordination number of $OPPh_3$ for the signal at 53.0 ppm was evaluated as 4.1 ± 0.1 from the peak integrals, indicating that this signal is assigned to

$UO_2(OPPh_3)_4^{2+}$. This shows good agreement with $UO_2(OPPh_3)_4^{2+}$ in [BMI][NfO] (Figures 1 and 4a). On this basis, the coordination number for the species corresponding to the signal at 41.4 ppm was derived as 5.0 ± 0.2 at $T \leq$ 238 K; that is, this signal is attributable to $UO_2(OPPh_3)_5^{2+}$. Since CD_2Cl_2 is a noncoordinating solvent, it is obvious that UO_2^{2+} exists as $UO_2(OPPh_3)_4^{2+}$ or $UO_2(OPPh_3)_5^{2+}$ in CD_2Cl_2 under the presence of free $OPPh_3$.

In Figure 3, peak areas of $UO_2(OPPh_3)_4^{2+}$, $UO_2(OPPh_3)_5^{2+}$, and free $OPPh_3$ show the T dependence. This is related with the equilibrium between $UO_2(OPPh_3)_4^{2+}$ and $UO_2(OPPh_3)_5^{2+}$ as follows.

$$UO_2(OPPh_3)_4^{2+} + OPPh_3 \overset{K_{45}}{\rightleftharpoons} UO_2(OPPh_3)_5^{2+} \quad (14)$$

$$K_{45} = \frac{[UO_2(OPPh_3)_5^{2+}]}{[UO_2(OPPh_3)_4^{2+}][OPPh_3]_{free}} \quad (15)$$

The K_{45} values at different T values were calculated from the peak integrals in Figure 3. The resulting values are plotted against T^{-1} in Figure S3 (Supporting Information) together with those under other $[OPPh_3]_{ini}$ conditions (9.80×10^{-3} and 3.57×10^{-2} M). It should be noted that free $OPPh_3$ is consumed to form $UO_2(OPPh_3)_5^{2+}$ (eq 14). Thus, true $[OPPh_3]_{free}$ is different from the initial one, when the presence of $UO_2(OPPh_3)_5^{2+}$ is significant. To distinguish them, the initial concentration of $OPPh_3$ is denoted by $[OPPh_3]_{ini}$. With the presence of free $OPPh_3$, $UO_2(OPPh_3)_4^{2+}$, and $UO_2(OPPh_3)_5^{2+}$ in CD_2Cl_2, $[OPPh_3]_{free}$ under each condition was calculated from the peak integrals in the corresponding ^{31}P NMR spectrum. Figure S3 shows that log K_{45} increases with an increase in T^{-1} (i.e., a decrease in T), indicating that $UO_2(OPPh_3)_5^{2+}$ is stabilized at low T. The formation enthalpy (ΔH_{45}) and entropy (ΔS_{45}) of eq 14 were evaluated as −57.8 ± 6.4 kJ mol^{-1} and −221 ± 32 J mol^{-1} K^{-1}, respectively, by using the van't Hoff relationship (eq S2, Supporting Information). At 298 K, log K_{45} is derived as −1.4 from the estimated thermodynamic parameters.

To our knowledge, the 5-fold complex, $UO_2(OPPh_3)_5^{2+}$, was reported first. The uranyl ion generally has three to six coordination sites in its equatorial plane. For small unidentate ligands (e.g., H_2O and dimethyl sulfoxide), the coordination number in the equatorial plane is generally 5, while it reduces to 4 for bulky ligands such as hexamethylphosphoramide[41,42] and $OPPh_3$.[28,29] Therefore, the equatorial plane of $UO_2(OPPh_3)_5^{2+}$ must be highly crowded. Nevertheless, $UO_2(OPPh_3)_5^{2+}$ exists as a major species at low T. This implies that UO_2^{2+} essentially prefers the pentagonal geometry in its equatorial plane. This character would be prevented by thermal motion of the bulky ligand, because the phenyl groups of the coordinated $OPPh_3$ in $UO_2(OPPh_3)_5^{2+}$ have to be highly ordered to reduce steric hindrance between them.

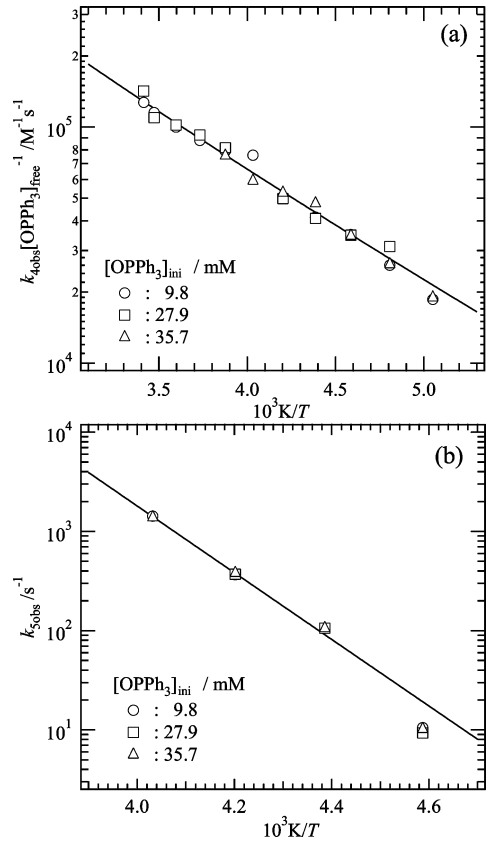

Figure 8. Temperature dependence of (a) $k_{4obs}[OPPh_3]_{free}^{-1}$ and (b) k_{5obs}. The smooth line is the best fit of the Eyring relationship (eq S1, Supporting Information) to the experimental data.

The broadening and coalescence of the signals of the free and coordinated $OPPh_3$ were also observed with changing T, indicating that the $OPPh_3$ exchange reactions of both 4- and 5-fold complexes occur in CD_2Cl_2, eqs 5 and 16:

$$UO_2(OPPh_3)_5^{2+} + OPPh_3^* \rightarrow UO_2(OPPh_3)_4(OPPh_3^*)^{2+} + OPPh_3 \quad (16)$$

where the asterisk on $OPPh_3$ is a typographical distinction only. Here, the apparent first-order rate constants of eqs 5 and 16 in CD_2Cl_2 are denoted by k_{4obs} and k_{5obs}, respectively. The T dependence of $k_{4obs}[OPPh_3]_{free}^{-1}$ and k_{5obs} is shown in Figure 8a and b, respectively. It must be noted that $[OPPh_3]_{free}$ at low T is different from that at high T because of the consumption of free $OPPh_3$ in the formation of $UO_2(OPPh_3)_5^{2+}$. Hence, k_{4obs} was divided by $[OPPh_3]_{free}$ for normalization.

In Figure 8a, any significant dependence of $k_{4obs}[OPPh_3]_{free}^{-1}$ on $[OPPh_3]_{free}$ was not observed despite 3.6-fold variation of $[OPPh_3]_{free}$. Therefore, k_{4obs} is written as the same formula as eq 6:

$$k_{4obs} = k_4[OPPh_3]_{free} \quad (17)$$

Thus, the reaction mechanism of eq 5 in CD_2Cl_2 should be categorized in the A mechanism. The rate-determining step of eq 5 in CD_2Cl_2 should also be eq 13.

(41) Fratiello, A.; Vidulich, G. A.; Cheng, C.; Kubo, V. *J. Sol. Chem.* **1972**, *1*, 433–444.
(42) Honan, G. J.; Lincoln, S. F.; Williams, E. H. *Inorg. Chem.* **1978**, *17*, 1855–1857.

In Figure 8b, k_{5obs} is independent of $[OPPh_3]_{free}$:

$$k_{5obs} = k_5 \quad (18)$$

where k_5 is the first-order rate constant of eq 16. This equation indicates that the rate-determining step of eq 16 is the dissociation of $OPPh_3$ from $UO_2(OPPh_3)_5^{2+}$ (eq 19), that is, the "dissociative" (*D*) mechanism.

$$UO_2(OPPh_3)_5^{2+} \xrightarrow{k_5} UO_2(OPPh_3)_4^{2+} + OPPh_3 \quad (19)$$

The activation parameters of eqs 5 and 16 in CD_2Cl_2 were derived from the least-squares fits of eq S1 to $k_{4obs}[OPPh_3]_{free}^{-1}$ ($= k_4$) and k_{5obs} ($= k_5$) in Figure 8. The results are $\Delta H_4^{\ddagger} = 7.1 \pm 0.3$ kJ mol^{-1} and $\Delta S_4^{\ddagger} = -122 \pm 1$ J mol^{-1} K^{-1} for k_4; $\Delta H_5^{\ddagger} = 62.4 \pm 1.0$ kJ mol^{-1} and $\Delta S_5^{\ddagger} = 68.4 \pm 4.2$ J mol^{-1} K^{-1} for k_5. The rate constants k_4 and k_5 at 298 K in CD_2Cl_2 were calculated from the activation parameters as 1.4×10^5 M^{-1} s^{-1} and 2.7×10^5 s^{-1}, respectively.

If the forward and reverse reactions of eq 14 simply follow eqs 13 and 19, respectively, K_{45} can be related with k_4 and k_5 as follows:

$$K_{45} = \frac{k_4}{k_5} \quad (20)$$

Thus, the thermodynamic parameters ΔH_{45} and ΔS_{45} are given by

$$\Delta H_{45} = \Delta H_4^{\ddagger} - \Delta H_5^{\ddagger} \quad (21)$$

$$\Delta S_{45} = \Delta S_4^{\ddagger} - \Delta S_5^{\ddagger} \quad (22)$$

The ΔH_{45} and ΔS_{45} calculated by eqs 21 and 22 are -55.3 ± 3.8 kJ mol^{-1} and -190 ± 5 J mol^{-1} K^{-1}, respectively. These values agree with the actual ΔH_{45} (-57.8 ± 6.4 kJ mol^{-1}) and ΔS_{45} (-221 ± 32 J mol^{-1} K^{-1}) within the error range. Therefore, it is concluded that eq 14 simply consists of eqs 13 and 19. This also verifies the validity of the mechanisms of the $OPPh_3$ exchange reactions in $UO_2(OPPh_3)_4^{2+}$ and $UO_2(OPPh_3)_5^{2+}$ in CD_2Cl_2.

3.4. Reactivity of $UO_2(OPPh_3)_n^{2+}$ in [BMI][NfO] versus CD_2Cl_2. Beside the ^{31}P NMR signals of free $OPPh_3$ and $UO_2(OPPh_3)_4^{2+}$ observed in [BMI][NfO], an additional signal for $UO_2(OPPh_3)_5^{2+}$ was observed in CD_2Cl_2. However, the presence of $UO_2(OPPh_3)_5^{2+}$ in CD_2Cl_2 was confirmed only at $T \leq 238$ K, where the [BMI][NfO] system cannot be studied because of solvent freezing. Therefore, we cannot compare the stability of $UO_2(OPPh_3)_5^{2+}$ between both solvents. The rate equations of the $OPPh_3$ exchange reactions of $UO_2(OPPh_3)_4^{2+}$ in both solvents were confirmed to be the same as each other (eqs 6 and 17). As shown in eq 13, the suggested A mechanism results in an intermediate with an additional $OPPh_3$, that is, $UO_2(OPPh_3)_5^{2+}$, which is detected in CD_2Cl_2 as a stable species at $T \leq 238$ K. Hence, the formation of $UO_2(OPPh_3)_5^{2+}$ as a short-lived intermediate in [BMI][NfO] should be reasonable.

The kinetic parameters of $UO_2(OPPh_3)_n^{2+}$ ($n = 4, 5$) in the different media are compared in Table 3. As a result, k_4 at 298 K in [BMI][NfO] is 1/20 times smaller than that in CD_2Cl_2. The $\Delta H_4^{\ddagger}$ value of eq 5 in [BMI][NfO] is also larger than that in CD_2Cl_2. Since the chemical species of interest in both systems are obviously the same, the difference in the reactivity of $UO_2(OPPh_3)_4^{2+}$ is considered to arise from the solvents.

Table 3. Kinetic Data of $OPPh_3$ Exchange Reactions of $UO_2(OPPh_3)_n^{2+}$ in [BMI][NfO] and CD_2Cl_2

solvent	n	$\Delta H_n^{\ddagger}$/kJ mol^{-1}	$\Delta S_n^{\ddagger}$/J mol^{-1} K^{-1}	k_n at 298 K/s^{-1}	mech.
[BMI][NfO]	4	55.3 ± 2.8	16.1 ± 7.9	7.2×10^3 M^{-1}[a]	A
CD_2Cl_2	4	7.1 ± 0.3	-122 ± 1	1.4×10^5 M^{-1}[a]	A
CD_2Cl_2	5	62.4 ± 1.0	68.4 ± 4.2	2.7×10^5	D

[a] Second-order rate constant.

One of the largest differences between [BMI][NfO] and CD_2Cl_2 is viscosity. According to Bonhote and co-workers,[6] the viscosity η of [BMI][NfO] at 293 K is 373 mPa s, while the η of CH_2Cl_2 is only 0.435 mPa s at the same T.[43] Thus, diffusion of the species in [BMI][NfO] will be much slower than that in CD_2Cl_2; that is, the reaction rate of eq 5 in [BMI][NfO] might be controlled by diffusion of the reactants. To make this point clear, a self-diffusion coefficient of BMI^+, D_{BMI}, in [BMI][NfO] was measured by means of the ^{1}H PGSE method. The resulting echo attenuation as a function of b in eq 4 is shown in Figure S4 (Supporting Information). From the best fit of eq 3 to the points in Figure S4, D_{BMI} was estimated as $(4.30 \pm 0.09) \times 10^{-12}$ m^2 s^{-1} at 297 K. Assuming that the diffusion coefficients of the reactants of eq 5 in [BMI][NfO] are equal to D_{BMI}, the k_4 in [BMI][NfO] at diffusion control (k_4^{dif}) is expressed as

$$k_4^{dif} = 4\pi d(2 \times D_{BMI})N_A \quad (23)$$

where d and N_A are the collision diameter and the Avogadro number, respectively.[44] From the crystallographic information of $UO_2(OPPh_3)_4^{2+}$, d was estimated as ca. 1×10^{-9} m. Using these parameters, k_4^{dif} in [BMI][NfO] was calculated as 7×10^7 M^{-1} s^{-1} at 297 K. On the other hand, the actual value of k_4 in [BMI][NfO] is 7.2×10^3 M^{-1} s^{-1} at 298 K, which is much smaller than k_4^{dif}. This indicates that the rate of eq 5 is kinetically controlled even in viscous [BMI][NfO].

In [BMI][NfO], the strong ionic atmosphere is formed, while CD_2Cl_2 is electrically neutral. Furthermore, $UO_2(OPPh_3)_4^{2+}$ is positively charged in both solvents. Therefore, it is predicted that $UO_2(OPPh_3)_4^{2+}$ is strongly solvated by NfO^- through a Coulombic interaction between the charged species. As a result, $UO_2(OPPh_3)_4^{2+}$ is largely stabilized in [BMI][NfO]. It should be emphasized that $UO_2(OPPh_3)_4^{2+}$ is not coordinated by NfO^- in [BMI][NfO] as described above. In the association of $OPPh_3$ to $UO_2(OPPh_3)_4^{2+}$ (eq 13), the entering $OPPh_3$ has to break this strong solvation barrier of NfO^- to reach $UO_2(OPPh_3)_4^{2+}$. In contrast, such a specific solvation will not occur in CD_2Cl_2. This may appropriately explain the difference in the reactivity of $UO_2(OPPh_3)_4^{2+}$ between [BMI][NfO] and CD_2Cl_2. The unique strong solvation around $UO_2(OPPh_3)_4^{2+}$ in [BMI][NfO] can also be supported by the difference in $\Delta S_4^{\ddagger}$ (16.1 ± 7.9 J mol^{-1} K^{-1} in [BMI][NfO] and -122 ± 1 J mol^{-1} K^{-1} in

(43) Acevedo, I. L.; Katz, M. *J. Solution Chem.* **1990**, *19*, 1041–1052.
(44) Moore, W. J. *Physical Chemistry*, 4th ed.; Prentice-Hall, Inc.: Englewood Cliffs, NJ, 1972; pp 416.

CD_2Cl_2). When the stronger solvation barrier around $UO_2(OPPh_3)_4^{2+}$ in [BMI][NfO] is broken, the solvation structure around the species in the activation process of eq 13 in [BMI][NfO] is disordered more largely than that in CD_2Cl_2. As a result, a larger $\Delta S_4^{\ddagger}$ was observed in [BMI][NfO].

4. Conclusion

In this study, we have investigated the complexation of UO_2^{2+} with $OPPh_3$ in [BMI][NfO] ionic liquid. As a result of the ^{31}P NMR spectrum, it was revealed that UO_2^{2+} is coordinated by $OPPh_3$ to form the 4-fold complex $UO_2(OPPh_3)_4^{2+}$, even in [BMI][NfO]. The structure of this $UO_2^{2+}-OPPh_3$ complex in [BMI][NfO] is considered to be similar to that determined from the single-crystal X-ray analysis of $UO_2(OPPh_3)_4(ClO_4)_2$ deposited from the same [BMI][NfO] solution. Furthermore, the $OPPh_3$ exchange reaction of $UO_2(OPPh_3)_4^{2+}$ in [BMI][NfO] was also studied using ^{31}P NMR spectroscopy. As a consequence, the apparent first-order rate constant k_{obs} of this reaction was found to be given by eq 6. From the discussion about the expression of k_{obs} and the exchange mechanism, the $OPPh_3$ exchange reaction of $UO_2(OPPh_3)_4^{2+}$ in [BMI][NfO] was classified in the "associative" (A) mechanism. The validity of the A mechanism was supported by finding the 5-fold complex, $UO_2(OPPh_3)_5^{2+}$, and its equilibrium with $UO_2(OPPh_3)_4^{2+}$ (eq 14) in CD_2Cl_2. The activation parameters of the $OPPh_3$ exchange reaction in [BMI][NfO] were also evaluated. Even in highly viscous [BMI][NfO], this ligand exchange reaction is not diffusion-controlled, but kinetically controlled. The reaction rate of the $OPPh_3$ exchange reaction of $UO_2(OPPh_3)_4^{2+}$ in [BMI][NfO] is much slower than that in CD_2Cl_2. As an explanation for the drastic difference in the reactivity of $UO_2(OPPh_3)_4^{2+}$ between [BMI][NfO] and CD_2Cl_2, the specific solvation of NfO^- around $UO_2(OPPh_3)_4^{2+}$ via Coulombic interaction between the charged species was suggested.

Acknowledgment. We thank Prof. Ingmar Grenthe for the stimulated discussion with him and his helpful advisees.

Note Added after ASAP Publication. Due to production errors, this article was published ASAP on January 12, 2009, with minor text errors. The corrected article was published ASAP on January 15, 2009.

Supporting Information Available: The Eyring and van't Hoff relationships, ^{31}P NMR spectra of free $OPPh_3$ in [BMI][NfO] and CD_2Cl_2, ORTEP drawing of $UO_2(OPPh_3)_4^{2+}$ in a perchlorate salt obtained from ethanol solution, temperature dependence of K_{45}, echo attenuation for [BMI][NfO] as a function of b at 297 K, and crystallographic information file of $UO_2(OPPh_3)_4(ClO_4)_2$ deposited from [BMI][NfO]. This material is available free of charge via the Internet at http://pubs.acs.org.

IC8018666